Journal of The Electrochemical Society, **162** (9) A1718-A1724 (2015)
0013-4651/2015/162(9)/A1718/7/$33.00 © The Electrochemical Society

Effect of a Size-Dependent Equilibrium Potential on Nano-$LiFePO_4$ Particle Interactions

Bernardo Orvananos,[a,*,e] Hui-Chia Yu,[a] Rahul Malik,[b] Aziz Abdellahi,[b] Clare P. Grey,[c,d,] Gerbrand Ceder,[b,**] and Katsuyo Thornton[a,**,z]**

[a]*Department of Materials Science and Engineering, University of Michigan, Ann Arbor, Michigan 48109, USA*
[b]*Department of Materials Science and Engineering, Massachusetts Institute of Technology, Cambridge, Massachusetts 02139, USA*
[c]*Department of Chemistry, University of Cambridge, Cambridge, CB2 1EW, United Kingdom*
[d]*Department of Chemistry, Stony Brook University, Stony Brook, New York 11794, USA*

Several electrode materials, such as $LiFePO_4$, have a thermodynamic driving force toward phase separation. However, phase separation inside the electrode particles can be suppressed when the particles are nanosized. In this case, each individual particle remains monophasic, but phase separation can occur between particles via Li redistribution. Here, we investigate the dynamics of Li redistribution when the equilibrium potential is size dependent. We perform simulations of the charge-discharge cycle in a two-particle cell and in a 65-particle agglomerate. The difference in particle equilibrium potentials can lead to an asymmetry between lithiation and delithiation of an electrode, in which the order of transformation of the particles during lithiation and delithiation is reversed. This effect is more significant at low currents but almost negligible at high currents.

Manuscript submitted February 25, 2015; revised manuscript received May 21, 2015. Published June 12, 2015.

$LiFePO_4$ (LFP) is a promising Li-ion battery material due to its thermal stability, long lifespan, and low toxicity.[1,2] As shown in experiments, LFP has a thermodynamic driving force toward phase separation.[3] However, it has been proposed that phase separation inside the particles ("intraparticle phase separation") may be prevented in nanoparticulate electrodes.[4–6] In this case, the particles remain monophasic, and instead Li can be redistributed between them to reduce their free energy and reach a stable state in a process we refer to as the "interparticle phase separation." This process has been the focus of several publications,[1,7–13] including our previous studies of particle-interaction dependence on particle position,[14] connectivity[15] and size.[15,16] The tendency for particles to remain monophasic leads to a discrete transformation of the particles at low currents.[7] This discrete transformation is believed to be responsible for several characteristics of LFP, such as a thermodynamic voltage hysteresis[7] and a memory effect.[17] It has been recently predicted that it also causes the current density at the particle surface to be nearly independent of cell C-rate.[13]

Particle size affects (de)lithiation dynamics in multiple forms. In the first form, as explored in our previous studies,[15,16] the surface-to-volume ratio difference allows smaller particles to reach the miscibility gap faster and to initiate interparticle phase separation. A second form is the difference in the equilibrium potential between particles of different radii. A dependence of the equilibrium potential on the particle size can stem from the difference in surface-to-volume ratio between particles of different sizes,[18] which causes the total surface-to-bulk free energy ratio to change with size. Another source of size dependence may be the change in stress in the host structure caused by the Gibbs-Thomson effect.[19,20] For LFP particles, several studies have suggested that smaller LFP particles exhibit higher equilibrium potentials than larger particles.[19,21]

In this study, we incorporate the dependence of the equilibrium potential on the particle size into our previously developed electrochemical model,[14–16] and use particle-level simulations to elucidate this additional effect on the dynamics of interparticle phase separation. For convenience we refer to this dependence as the "size effect." Two configurations are used for the simulations. The first is a configuration consisting of two particles of different sizes, and the second configuration is an agglomerate with 65 particles with a log-normal particle size distribution. Using these cell configurations, we simulate three cases: a lithiation-delithiation cycle at a low current and delithiation at two higher currents. These simulations will demonstrate that the effect of size-dependent equilibrium potential is significant at low rates and is insensitive at high rates. In addition, we present a derivation for calculating the current at which particles of two sizes react simultaneously, given the size-dependent equilibrium potential.

Model

Four governing equations are employed to model the physical mechanisms involved in the charge/discharge of the cell: the concentration evolution in (1) the particles and (2) electrolyte, (3) charge conservation in the electrolyte, and (4) reaction at the particle-electrolyte interfaces. For simplicity, we assume a uniform electrostatic potential between the particles and the cathode current collector, which is reasonable for the small size of the cells. We here use the Smoothed Boundary Method (SBM)[22–24] to incorporate the boundary conditions (including the interfacial reactions) into the partial differential equations to be solved. In the SBM, a domain parameter, ψ, is employed to represent the different domains. In this case $\psi = 1$ represents the particle domain, $\psi = 0$ the electrolyte domain, and $0 < \psi < 1$ the particle-electrolyte interface.

As in our previous publications,[14,15] we here assume that the particles transform through a metastable solid solution,[4] an assumption that has been recently validated experimentally.[12,25] The concentration evolution of the monophasic particles is modeled with Fick's diffusion.[16] The SBM form of Fick's diffusion equation can be written as

$$\frac{\partial C_p}{\partial t} = \frac{D_p}{\psi}\left[\nabla\cdot(\psi\nabla C_p)\right] + \frac{|\nabla\psi|}{\psi} r_{Li}, \qquad [1]$$

where C_p is the concentration of Li in the particles, D_p is the diffusivity, t is time, and r_{Li} is the reaction rate.

The dilute binary solution theory is utilized to model the electrolyte.[26] The SBM form of the concentration evolution in the electrolyte can be written as

$$\frac{\partial C_e}{\partial t} = \frac{D_{amb}}{1-\psi}\left[\nabla\cdot\left((1-\psi)\nabla C_e\right)\right] - (1-t_+)\frac{|\nabla\psi|}{1-\psi} r_{Li}, \qquad [2]$$

where C_e is the salt concentration in the electrolyte, D_{amb} is the ambipolar diffusivity, and t_+ is the transference number of the cation. For the charge conservation in the electrolyte, the SBM equation is

*Electrochemical Society Student Member.
**Electrochemical Society Active Member.
[e]Present address: Department of Materials Science and Engineering, Massachusetts Institute of Technology, Cambridge, Massachusetts 02139, USA.
[z]E-mail: kthorn@umich.edu

the following:

$$\nabla \cdot \left[(1-\psi)\frac{F}{RT}(z_+ D_+ - z_- D_-) C_e \nabla \phi_e \right] = |\nabla \psi| \frac{r_{Li}}{\upsilon_+} + \nabla \cdot [(1-\psi)(D_- - D_+)\nabla C_e], \quad [3]$$

where F is Faraday's constant, R is the ideal gas constant, T is temperature, ϕ_e is the electrostatic potential in the electrolyte, and υ_+ is the dissociation number of the cation. Furthermore, z_i and D_i are the charge number and the diffusivity for species i.

The electrochemical reaction rate is calculated using the Butler-Volmer equation,

$$r_{Li} = \frac{i_0}{F}\sqrt{\frac{C_e}{C_e^0}}\left[\exp\left(-\frac{\alpha F}{RT}\eta \right) - \exp\left(\frac{(1-\alpha)F}{RT}\eta \right) \right], \quad [4]$$

where i_0 is the exchange current density, C_e^0 is the reference average Li concentration in the electrolyte for the experimental system in which the exchange current density is measured, and α is the transfer coefficient. The overpotential η is defined as

$$\eta = \Delta\phi - \phi_{eq}(r), \quad [5]$$

where $\Delta\phi = \phi_p - \phi_e$ is the electrostatic potential difference across the particle-electrolyte interface and ϕ_p is the electrostatic potential in the particles. $\phi_{eq}(r)$ is the size-dependent equilibrium potential. Note that $\Delta\phi$ is nearly equal to the cell voltage because of the small cell size, limited C-rates, and because no other losses are considered. Ignoring nanoscale effects, we model the size effect as inversely proportional to the particle radius as in Ref. 18. Here, $\phi_{eq}(r)$ is defined as a function of the particle radius, r, according to the size effect:

$$\phi_{eq}(r) = \phi_{eq}^0 + \frac{a}{r}, \quad [6]$$

where a is a constant quantifying the magnitude of the size effect. Furthermore, ϕ_{eq}^0 is the equilibrium potential of an infinitely large particle, defined by the polynomial[15]

$$\phi_{eq}^0 = \left\{ V_{OC} + \left[5(1.05 - 2.1X_p)^{51} - 2.925275X_p^2 + 6.375071X_p - 2.558325 \right] \times 10^{-2} \right\} [\mathrm{V}], \quad [7]$$

where V_{OC} is the reference open circuit voltage plateau, $X_p = C_p\Omega$, and Ω is the molar volume of LFP. As can be inferred from Eq. 6, the size effect is significant when the particle radius is small. Here, we consider a metastable solid-solution model in which Li concentration remains nearly uniform throughout the bulk and surfaces of the particles, which justifies the constant shift of the equilibrium potential due to the size effect.

The value of a is 1.7×10^{-8} V/cm, which is estimated from the results reported by Meethong et al.[19] based on a difference of 7 mV in the open circuit voltage of 17-nm- and 56.5-nm-radius particles. If the source of the size effect were solely attributed to the surface-to-volume ratio of the particles, as in Ref. 18, the value of a we selected would correspond to a value of $\sigma_{LFP} - \sigma_{FP} = -1.2 \times 10^{-5}$ J/cm^2. Here σ_{LFP} and σ_{FP} are the surface free energies of $LiFePO_4$ and $FePO_4$, respectively. Note that a is an empirical parameter combining the contribution from various surface orientations present; ab initio calculations indicate that the size effect would be negative for the (010) surface and larger for the remainder of the surfaces.[18,27]

The values of D_p, D_+ and D_- are set to 5×10^{-13} cm^2/s (comparable to the values from Refs. 28, 29), 7.3×10^{-7} cm^2/s (Ref. 30) and 1.5×10^{-6} cm^2/s,[30] respectively. The electrolyte has an initial concentration of 1 M. The temperature is set to 300 K, V_{OC} to 3.42 V (Ref. 3), i_0 to 8.5×10^{-7} A/cm^2,[15] and Ω to 43.86 cm^3/mol. A constant-current and a no-flux boundary conditions are imposed at the anode-electrolyte and the electrolyte-current collector interfaces, respectively. For the remainder of the box boundaries, a no-flux and a periodic boundary conditions are imposed for the two-particle cell and the agglomerate, respectively. A central finite difference scheme is used for the spatial discretization with a 2-nm and 2.5-nm spacing for the two-particle and the 65-particle configurations, respectively. Eq. 1 is solved explicitly using an Euler time stepping scheme; Eqs. 2 is solved implicitly using and alternating-direction-line-relaxation (ADLR)[23,31,32] method. The solution for Eq. 3 is also obtained by ADLR every time step.

Results

The results for the two-particle and the 65-particle configurations are now described. We only show the results for the particle concentration evolution and the cell voltage, as the electrostatic potential and salt concentration in the electrolyte are nearly uniform due to the small dimension of the cells.

Two-particle configuration.— In this section, we use a cell configuration identical to that used in our previous work,[16] containing two particles of different sizes. The smaller particle has a 40-nm diameter, and the larger particle has a 70-nm diameter. The dimensions of the domain are $96 \times 180 \times 96$ nm^3. Figure 1a shows this configuration, which also denotes the locations of the anode and current collector.

We first simulate the lithiation-delithiation cycle at $\bar{i} = 6\% i_0$ (i.e, the average current at the particle surface is equivalent to 6% of the value of i_0). This current density corresponds to C/12.5 for this cell. Figure 2a shows the depth of discharge (DOD) for the particles and cell during lithiation. The corresponding voltage is plotted in Fig. 2c curve (i) with the single-particle equilibrium potentials of the two particles. The size effect produces a higher particle equilibrium potential for the smaller particle, as shown by the black dotted curve in Fig. 2c. The driving force for lithiation is $\phi_{eq}(r) - \Delta\phi = -\eta$. Thus, the size effect enhances lithiation of the smaller particle by increasing $\phi_{eq}(r)$, and consequently the driving force, which further facilitates interparticle phase separation. In addition to this enhancement, the general lithiation dynamics remain similar to the case in which the size effect is excluded, which are shown in Figs. 2d (DOD) and 2f curve (i) (voltage). This case was described in our previous study,[16] in which we provided a step-by-step explanation of the relationship between the sudden changes of the cell voltage and the equilibrium potential of each particle; therefore, we do not repeat it here.

The size effect significantly affects the delithiation dynamics at low currents. Figure 1 shows the concentration evolution of the particles during delithiation. Initially, both particles are nearly fully lithiated. At $\bar{i} = 6\% i_0$, the smaller particle remains lithium-rich until the larger particle becomes nearly fully delithiated; see Figs. 1b and 1c. When the larger particle is fully delithiated, the smaller particle begins delithiation; see Fig. 1d.

Figures 2b and 2c curve (ii) show the DOD of the particles and voltage, respectively, for delithiation at $\bar{i} = 6\% i_0$. Note that the abscissa in Fig. 2b is the state of charge (SOC = 1-DOD). At the beginning of delithiation, the cell voltage enters the range between the equilibrium potential of the larger particle (solid black curve in Fig. 2c) and the smaller particle (dotted black curve in the same figure). The driving force for delithiation is $\Delta\phi - \phi_{eq}(r) = \eta$. Therefore, the size effect reduces the driving force for delithiation for the smaller particle. In the case presented in Figs. 2b and 2c, only the larger particle is

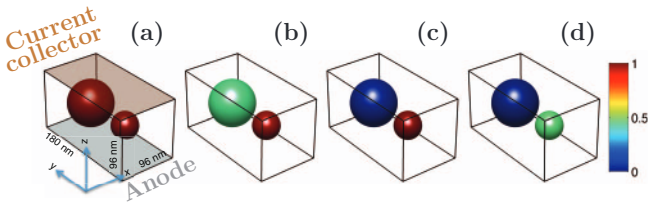

Figure 1. Concentration evolution of the two-particle configuration during delithiation at $\bar{i} = 6\% i_0$. Four snapshots of the process are shown at different cell depths of discharge (DODs): (a) 98% (initial concentration), (b) 54%, (c) 19%, and (d) 10%. The colors in the color bar represent x in Li_xFePO_4. A schematic of the configuration is included in (a).

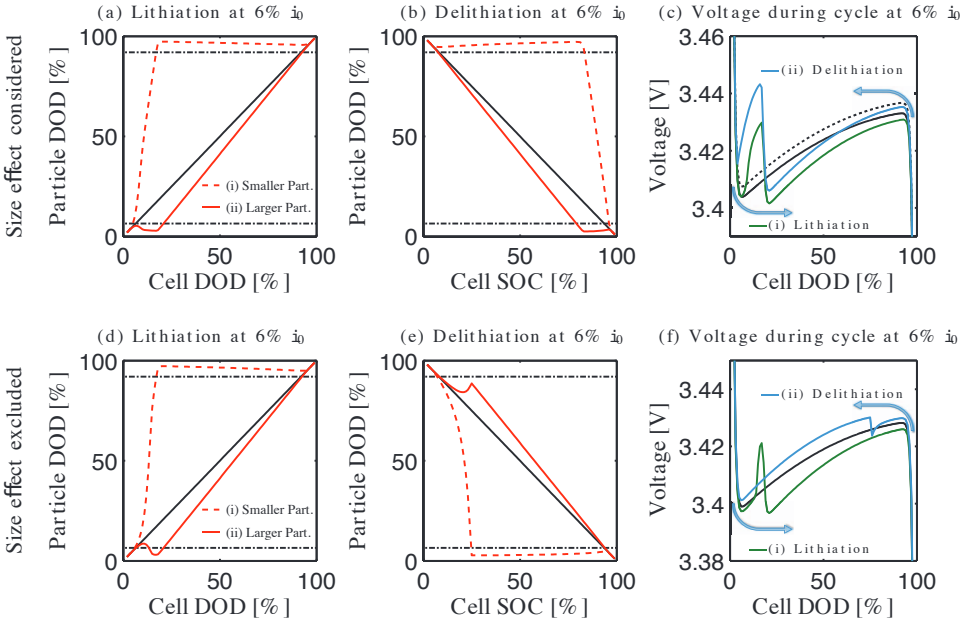

Figure 2. The particle DOD and voltage of the two-particle configuration during a lithiation-delithiation cycle at $\bar{i} = 6\%i_0$ when the size effect is (a)-(c) considered and (d)-(f) excluded from the calculation. In (a), (b), (d), and (e), the black solid line represents the cell DOD, and the horizontal dash-dotted line represents the spinodal points. In (c), the solid and dotted black curves indicate the equilibrium potential of the larger and smaller particles, respectively; in (f), the solid curve indicates the size-independent equilibrium potential. The horizontal axis in (b) and (e) is the state of charge (SOC = 1-DOD).

driven by the cell voltage to delithiate for the given current. As the larger particle delithiates, the cell voltage decreases further. Thus, the smaller particle remains nearly fully lithiated. When the larger particle is nearly fully delithiated, the cell voltage increases above the smaller particle equilibrium potential at its upper spinodal point (the local maximum of the equilibrium potential) to maintain the current, causing the smaller particle to begin delithiating. When the size effect is excluded from the model, as shown in Fig. 2e and 2f curve (ii), the smaller particle reacts first due to its greater surface-to-volume ratio. The difference between lithiation and delithiation when the size effect is excluded is due to asymmetric equilibrium potential. The smoother shape of the equilibrium potential at the upper spinodal point weakens the interparticle interactions. The size effect enhances the asymmetry in the lithiation/delithiation dynamics by favoring the delithiation of the larger particle.

To further investigate the size effect during delithiation, simulations were performed at two additional currents: $\bar{i} = 18\%i_0$ (C/4.2 rate) and $54\%i_0$ (C/1.4 rate). (No additional simulations were performed for lithiation because it does not exhibit major differences from the case without the size effect.) The results are shown in Fig. 3. A higher current produces a higher overpotential and, consequently, a higher cell voltage. At $i = 18\%i_0$, the voltage is sufficiently high such that it exceeds the equilibrium potential of the smaller particle at its upper spinodal point, which facilitates delithiation of both particles at the beginning of the process. However, the larger particle reacts more rapidly than the smaller particle due to the larger overpotential. The voltage decreases as the larger particle delithiates because of its decreasing equilibrium potential. Eventually, the applied potential becomes lower than the equilibrium potential of the smaller particle, which causes the smaller particle to lithiate again to a nearly fully lithiated state. The remaining dynamics proceeds in a similar manner as at $\bar{i} = 6\%i_0$. At the highest current considered, $\bar{i} = 54\%i_0$, the overpotential is sufficiently large such that the size effect is negligible. The voltage is higher than the equilibrium potentials of both particles throughout the entire delithiation process, and the smaller particle delithiates more rapidly than the larger particle due to its larger surface-to-volume ratio.

In this simplified configuration, it is possible to derive an applied current at which the two particles can delithiate at the same rate, even when the two spherical particles have different radii. Here, we assume that transport is not limited (in both the particles and electrolyte) and that the electrostatic potential distribution is uniform throughout the

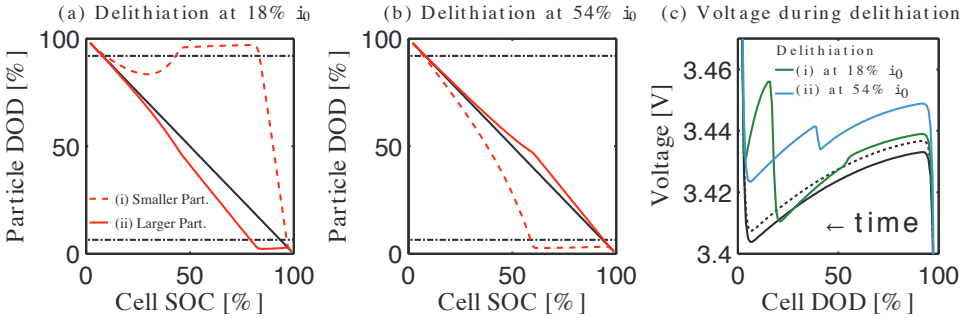

Figure 3. The particle DOD and voltage for the two-particle configuration during delithiation at (a) $\bar{i} = 18\%i_0$ and (b) $\bar{i} = 54\%i_0$. In (a) and (b), the black solid line represents the cell DOD, and the horizontal dash-dotted line represents the spinodal points. In (c), the solid and dotted black curves indicate the equilibrium potential of the larger and the smaller particles, respectively. The horizontal axis in (a) and (b) is the SOC. Note that in (c) the time increases toward the left.

cell. The two particles will delithiate at the same current per volume (proportional to the C-rate) if the particle current normalized by the particle volume is identical:

$$i_1 \frac{A_1}{V_1} = i_2 \frac{A_2}{V_2}, \quad [8]$$

where i_j, A_j and V_j are the particle current density, surface area and volume, respectively, of particle j. At a low current, it is a reasonable approximation to linearize the Butler-Volmer equation, which allows us to obtain the current densities at the particles' surfaces as follows.

$$i_1 = -\frac{Fi_0 a}{RTr_2} \quad \text{and} \quad i_2 = -\frac{Fi_0 a}{RTr_1}. \quad [9]$$

See Appendix for derivation of Eq. 9. We calculate the average current density (total current/total particle surface) as

$$\bar{i}(A_1 + A_2) = i_1 A_1 + i_2 A_2. \quad [10]$$

The expressions for i_1 and i_2 from Eq. 9 are substituted into Eq. 10 to obtain the following,

$$\bar{i} = -\frac{Fi_0 a}{RTr_1 r_2} \frac{\left(r_1^3 + r_2^3\right)}{\left(r_1^2 + r_2^2\right)}. \quad [11]$$

Equation 11 is also applicable to a cell containing particles of two different sizes that are evenly distributed between the two sizes with the same number of particles of each size. This equation can be easily generalized to account for different number of particles in each size group.

In our aforementioned simulations, the order of delithiation of the particles changed between $\bar{i} = 18\% i_0$ and $\bar{i} = 54\% i_0$. According to Eq. 11, the transition should occur at $\bar{i} = 29.4\% i_0$. To verify this prediction, we performed several simulations with applied currents of various magnitudes at approximately $\bar{i} = 29.4\% i_0$. The transition occurred at applied currents between $\bar{i} = 27.9\% i_0$ and $\bar{i} = 28.8\% i_0$. The small discrepancy between the prediction and simulation is attributed to the approximations in the derivation of Eq. 11 (including linearization of the Butler-Volmer equation) and the error in the simulation associated with the finite thickness of the SBM interface.[23]

Dilute agglomerate configuration.— The lithiation-delithiation dynamics for a cell containing 65 particles are now discussed. The particles are randomly distributed throughout the 320 × 320 × 300 nm^3 domain without allowing the particles to contact one another. An empty region was left in the bottom 30 nm of the domain, which corresponds to the separator. The particles follow a log-normal size distribution, f, with a probability density function:

$$f_{\tilde{a},\sigma,b,\beta}(r) = \begin{cases} \frac{1}{\sigma(r-b)\sqrt{2\pi}} \exp\left(-\frac{[\ln((r-b)/\beta)-\tilde{a}]^2}{2\sigma^2}\right) & \text{if } r > b \\ 0 & \text{if } r \le b, \end{cases} \quad [12]$$

where r is the radius of the particle (in nanometers), $\tilde{a} = 1$, $\sigma = 0.2$, $b = 5$ nm, and $\beta = 7.5$ nm.[15] The particle radii range approximately from 19 nm to 35 nm, with an average of 26 nm. The configuration is presented in Fig. 4a and is identical to the configuration used in our previous study.[15] Similar to the two-particle configuration, we first describe the lithiation-delithiation cycle at a low current followed by delithiation at two additional currents.

The simulation is performed at $\bar{i} = 6\% i_0$ (equivalent to C/11.1 rate for this case). Regarding lithiation, Figs. 5a and 5c curve (i) show the DOD of the 65 particles, arranged in the order of their size, and cell voltage, respectively. The single-particle equilibrium potentials of the second-smallest (r = 18.7 nm) and second-largest (r = 35 nm) particles are also shown in Fig. 5c. Here, we selected the second-smallest and the second-largest particles and not the smallest/largest because the smallest/largest particles are outliers of the distribution due to the statistically small number of the particles. As in the two-particle configuration, the lithiation dynamics in this simulation are similar to the case in which the size effect is excluded (discussed above and shown in Figs. 5d and 5f curve (i)); the only difference is that interparticle phase separation is enhanced. Lithiation begins with the smaller particles, and group-by-group sequential transformation occurs from the smaller to larger particles. During this lithiation process, the cell voltage exhibits a series of discrete (in this case five) sudden increases and decreases that correspond with the group-by-group transformation of the particles. This behavior has been described in detail in Ref. 15, and therefore it is not repeated here.

By contrast, during delithiation, the size effect facilitates delithiation of the larger particle via the equilibrium potential shift as discussed for the two-particle case. Figure 4 shows the concentration evolution of the particles during delithiation. As in the two-particle case, the larger particles delithiate first at low currents. Figures 5b and 5c curve (ii) show the DOD of the particles arranged by size and the resulting voltage for delithiation. As with lithiation, the particles react in groups, which produces sudden decreases and increases in the cell voltage. However, when the size effect is included, delithiation begins with the group of larger particles, unlike the case without the size effect, as shown in Figs. 5e and 5f curve (ii). An extended analysis of the mechanism underlying the group-by-group transformation is presented in Ref. 14. As with the two-particle configuration, the difference between lithiation and delithiation dynamics without the size effect is due to the asymmetric single-particle equilibrium potential.

Van der Ven and Wagemaker[18] suggested that there should be a slight overall tilt in the cell voltage due to the size effect. The simulation result in Fig. 5c appears to show this tilt, but it is not obvious due to the tight size distribution we employed and the small value of the constant a. A larger size dependence and/or a wider particle size distribution will enhance the tilt of the voltage curve.

The delithiation results for two additional currents are described below. The DOD of the particles during delithiation at $\bar{i} = 18\% i_0$ (C/3.7 rate) and $\bar{i} = 54\% i_0$ (C/1.2 rate) are shown in Figs. 6a and 6b, respectively. At $\bar{i} = 18\% i_0$, the larger particles react first, and the particles react in two groups. Many smaller particles undergo partial lithiation at the cell SOC between 25% and 50%. The results indicate that the size effect remains significant at this current. The cell voltage at this current is plotted as curve (i) in Fig. 6c. Two sudden decreases in the voltage curve are apparent and correspond to the group-by-

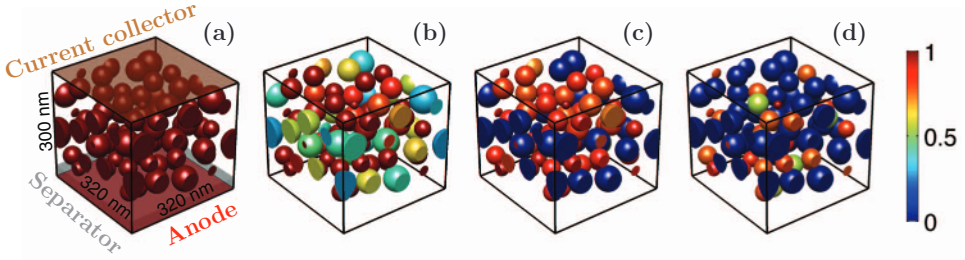

Figure 4. Concentration evolution of the dilute agglomerate during delithiation at $\bar{i} = 6\% i_0$. Snapshots of the process are shown at four different cell DODs, (a) 98% (initial concentration), (b) 71%, (c) 47%, and (d) 22%. A schematic of the configuration is included in (a).

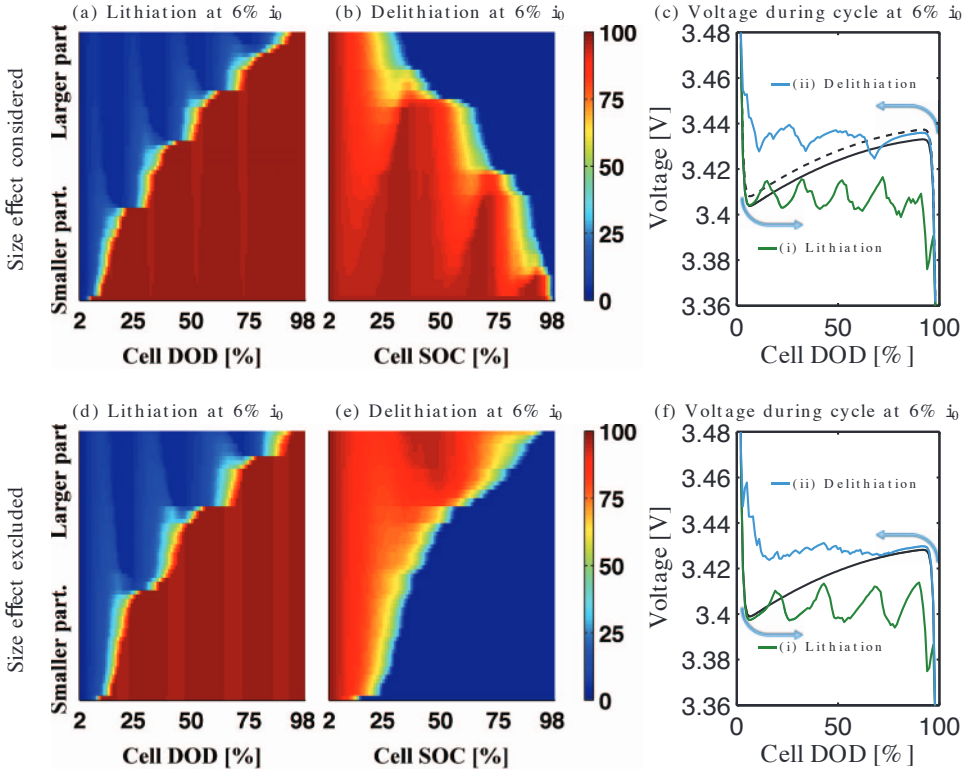

Figure 5. The particle DOD and voltage of the dilute agglomerate during a lithiation-delithiation cycle at $\bar{i} = 6\%i_0$ when the size effect is (a)-(c) considered and (d)-(f) excluded. In (a), (b), (d) and (e), the particles are arranged along the vertical axes according to their size, the bottom being the smallest particle and the top being the largest particle. The colors indicate the particle DOD according to the color bar on the right. Note that the horizontal axes in (b) and (e) are SOC. In (c), the solid and dotted black curves indicate the equilibrium potential of the second-largest and the second-smallest particle, respectively, as a function of the particle DOD (rather than the cell DOD). In (f) the solid curve indicate the size-independent equilibrium potential.

group interparticle phase separation events. At the early stage, almost all particles are delithiating because the cell voltage is higher than their single-particle equilibrium potentials, as shown in curve (i) at the cell DOD between 50% and 95% in Fig. 6c. The delithiation overpotential of the larger particles is much larger than that of the smaller particles. Thus, the larger particles delithiate more rapidly than the smaller particles, even though the smaller particles have a larger surface-to-volume ratio. At the higher current, $\bar{i} = 54\%i_0$, the voltage is sufficiently high such that the size effect is negligible; thus, the smaller particles delithiate first, unlike the previous case. Here, the smallest particle is abnormally small, and thus, the overwhelming size effect hinders its delithiation until all other particles are fully delithiated. In addition, the $\bar{i} = 54\%i_0$ voltage is sufficiently high such that interparticle phase separation is hindered,[16] and thus, all particles are delithiated nearly simultaneously. Therefore, the particles do not transform in groups.

Discussion

In portable electronics, intermittent rests during charge/discharge processes (delithiation/lithiation) are common. Because Li transport from/to the counter-electrode is halted, relaxation through interparticle phase separation is the only route toward equilibrium when intraparticle phase separation is suppressed. Although the size effect may

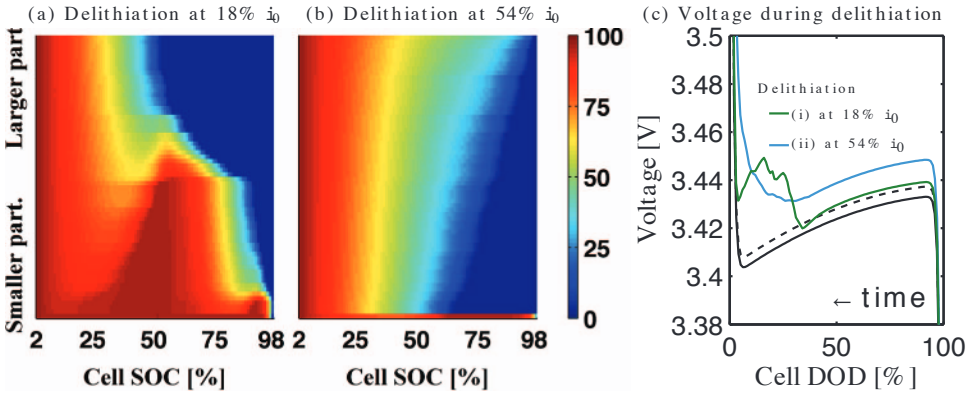

Figure 6. The particle DOD and voltage of the dilute agglomerate during delithiation at two additional currents: (a) $\bar{i} = 18\%i_0$ and (b) $\bar{i} = 54\%i_0$. In (c), the solid and dotted black curves indicate the equilibrium potential of the second-largest and second-smallest particles, respectively, as a function of the particle DOD (rather than the cell DOD). The horizontal axis in (a) and (b) is the SOC (1-DOD). Note that in (c) the time increases toward the left.

be small, it may be important for determining how phase separation proceeds. Under the assumption that smaller particles have a higher equilibrium potential, smaller particles will favor Li absorption from neighboring larger particles. During delithiation at a higher C-rate, where the size effect is negligible, the smaller particles delithiate before the larger particles. The smaller particles provide a better rate performance in comparison to the larger particles due to their larger surface-to-volume ratio. Thus, the rate performance of the cell will deteriorate as the smaller particles become fully delithiated and the current is supplied mostly by the larger particles. However, this deterioration may be avoided by a pause in the charge process because some of the smaller particles may draw Li from neighboring larger particles during the pause. The delithiation may then proceed similarly as the beginning of the delithiation process, in which the smaller particles delithiate before the larger particles. This process repeats with each pause during the charge process. By contrast, during lithiation the rate performance will degrade by intermittent rests. The smaller particles (which lithiate before the larger particles during discharge) continue to lithiate during the rest periods, extracting Li from the larger particles. Thus, the remainder of the process must proceed through insertion into the larger particles, which requires a larger overpotential for a given rate.

Synthesizing LFP cells with a narrow particle-size distribution can help spatially homogenize the reaction of the particles. However such a task can be challenging and expensive. Instead, for specific battery applications, an alternative approach to improve cell performance can be pursued. Due to the size effect, a particle-size distribution can be optimized to homogenize the charge over a cell for a given C-rate. Equivalently, for a given particle-size distribution, an optimal C-rate can be determined at which the particles delithiate homogeneously (again assuming that the smaller particles have a higher equilibrium potential). However, this type of optimization is only desirable for devices in which charge efficiency is more important than discharge efficiency and that are always charged at the same C-rate.

If the larger particles have a higher equilibrium potential, in contrast to the assumption herein, the changes in dynamics due to the size effect would be opposite of what has been described above. The size effect would favor larger particles for lithiation and smaller particles for delithiation and thus would not significantly affect delithiation behavior. However, the lithiation behavior could be reversed such that larger particles would lithiate before smaller particles. For this case, intermittent rest would be beneficial for lithiation (i.e., discharge) and detrimental for delithiation (i.e., charge). In such a case, the size effect can be exploited to enhance the rate performance in applications that have intermittent discharge. Candidate materials can thus be screened for their surface energies, in addition to voltage, thermal stability, diffusivity, etc.

Experimental batteries contain numerous particles with usually a wide size distribution. In such cells, small particles that remain monophasic coexist with two-phase large particles. As described in our previous work,[16] the particles that undergo intraparticle phase separation may react prior to monophasic particles of smaller size. The sequential group-by-group transformation dynamics observed in this work is not affected by the phase separation of large particles. However, the presence of many particles causes the discrete events of Li redistribution to occur at different times in different locations throughout the cathode.[15] Thus, in cells with many particles the oscillations in the cell voltage are no longer observable,[7] even though the consequence of such transformation mechanism still remains. It is also important to note that the tendency for the smaller/larger particles to favor lithiation/delithiation during rest periods also remains, even if the larger particles are phase separated.

Experiments can be designed to examine the predictions described above. For example, experimental comparisons between different C-rates could verify the prediction that larger particles delithiate before the smaller ones at a sufficiently low C-rate while, at a rate higher than a threshold, smaller particles delithiate before the larger ones. However, these experiments must be carefully designed such that the current densities at the particles' surfaces are well controlled. For example, Ref. 13 predicts that current density of the reacting particles is nearly constant when a cell consists of many particles. Therefore, the experiments may require a use of cells with a small number of particles. Also note that the presence of both two-phase and monophasic particles can lead to the change in the sequence of reaction,[16] and therefore the particle size and distribution should also be chosen to avoid this situation. These comparisons could be performed using nuclear magnetic resonance (as in Ref. 33), energy-dispersive X-ray diffraction (as in Refs. 34, 35), or synchrotron-based X-ray microscopy (as in Ref. 13).

Conclusions

In summary, we analyzed the size effect on lithiation/delithiation of particles in which intraparticle phase separation is suppressed. We first simulated a simple two-particle configuration to systematically analyze the size effect and derive the condition for concurrent delithiation of different-size particles. This was followed by the analysis of the size effect on a group of particles by simulating a system of a 65-particle agglomerate. We demonstrated that, when the smaller particles have a higher equilibrium potential, as suggested by experimental observations, the size effect does not lead to qualitative changes in the lithiation process. On the contrary, the size effect can reverse the order of particle phase transformation at low currents during delithiation. At higher currents, the size effect is negligible even during delithiation. The role of intermittent rests during the charge and discharge process was also discussed. We showed that charge rate performance could be enhanced with intermittent rests if the smaller particles have a higher equilibrium potential than the larger ones. This provides an additional material selection criterion for the cathode material selection, particularly for applications where charge rate performance is important.

Acknowledgments

We thank H. Liu and F. Strobridge for their valuable comments. This work was supported by the NorthEast Center for Chemical Energy Storage, an Energy Frontier Research Center funded by the U.S. DOE, Basic Energy Science under award numbers DE-SC0001294 and DE-SC0012583. Computational resources were provided by the Extreme Science and Engineering Discovery Environment (XSEDE) (allocation No. TG-DMR110007), which is supported by National Science Foundation grant number OCI-1053575, and local computational resources were provided by the University of Michigan Advanced Research Computing.

Appendix: Derivation of Eq. 9

We begin with the linearized Butler-Volmer equation:

$$i = -i_0 \left(\frac{F}{RT} \eta \right), \quad [A1]$$

where η is defined as

$$\eta = \Delta\phi - \left[\phi^0_{eq} + \frac{a}{r} \right]. \quad [A2]$$

When two particles react at the same C-rate, their surface current per volume is as follows:

$$i_1 \frac{A_1}{V_1} = i_2 \frac{A_2}{V_2}. \quad [A3]$$

For spherical particles, Eq. A3 can be rewritten as

$$\frac{i_1}{r_1} = \frac{i_2}{r_2}. \quad [A4]$$

Substituting Eq. A1 into Eq. A4 and reorganizing the equation, we obtain the following:

$$\frac{\eta_1}{r_1} = \frac{\eta_2}{r_2}. \quad [A5]$$

Using the definition from η (Eq. 5) and defining $\eta^0 = \Delta\phi - \phi^0_{eq}$ we can express Eq. A5 as follows:

$$\frac{1}{r_1} \left(\eta^0 - \frac{a}{r_1} \right) = \frac{1}{r_2} \left(\eta^0 - \frac{a}{r_2} \right), \quad [A6]$$

and we can solve for η^0,

$$\eta^0 = a\frac{r_2^2 - r_1^2}{r_1 r_2^2 - r_2 r_1^2}. \quad [A7]$$

Using Eq. A1 and Eq. A2, we can also write η^0 as a function of i and r for either particle as follows:

$$\eta^0 = -\left(\frac{i_2}{i_0}\frac{RT}{F}\right) + \frac{a}{r_2}. \quad [A8]$$

Equating Eq. A7 with A8 and solving for i_2, we obtain

$$i_2 = -\frac{Fi_0 a}{RTr_1}. \quad [A9]$$

Following the above derivation, we obtain i_1, as shown in Eq. 9.

References

1. R. Malik, A. Abdellahi, and G. Ceder, A Critical Review of the Li Insertion Mechanisms in $LiFePO_4$ Electrodes, *J. Electrochem. Soc.*, **160**(5), A3179 (2013).
2. Y. Wang, P. He, and H. Zhou, Olivine $LiFePO_4$: development and future, *Energy Environ. Sci.*, **4**(3), 805 (2011).
3. A. Yamada, H. Koizumi, S.-I. Nishimura, N. Sonoyama, R. Kanno, M. Yonemura, T. Nakamura, and Y. Kobayashi, Room-temperature miscibility gap in Li_xFePO_4, *Nat. Mater.*, **5**(5), 357 (2006).
4. R. Malik, F. Zhou, and G. Ceder, Kinetics of non-equilibrium lithium incorporation in $LiFePO_4$, *Nat. Mater.*, **10**(8), 587 (2011).
5. P. Bai, D. A. Cogswell, and M. Z. Bazant, Suppression of Phase Separation in $LiFePO_4$ Nanoparticles During Battery Discharge, *Nano Lett.*, **11**(11), 4890 (2011).
6. D. A. Cogswell and M. Z. Bazant, Coherency Strain and the Kinetics of Phase Separation in $LiFePO_4$ Nanoparticles, *ACS Nano*, **6**(3), 2215 (2012).
7. W. Dreyer, J. Jamnik, C. Guhlke, R. Huth, J. Moškon, and M. Gaberšček, The thermodynamic origin of hysteresis in insertion batteries, *Nat. Mater.*, **9**(5), 448 (2010).
8. W. Dreyer, C. Guhlke, and R. Huth, The behavior of a many-particle electrode in a lithium-ion battery, *Physica D*, **240**(12), 1008 (2011).
9. S. Dargaville and T. W. Farrell, A comparison of mathematical models for phase-change in high-rate $LiFePO_4$ cathodes, *Electrochim. Acta*, **111**, 474 (2013).
10. T. R. Ferguson and M. Z. Bazant, Nonequilibrium Thermodynamics of Porous Electrodes, *J. Electrochem. Soc.*, **159**(12), A1967 (2012).
11. T. R. Ferguson and M. Z. Bazant, Phase Transformation Dynamics in Porous Battery Electrodes, *Electrochim. Acta*, **146**(0), 89 (2014).
12. H. Liu, F. C. Strobridge, O. J. Borkiewicz, K. M. Wiaderek, K. W. Chapman, P. J. Chupas, and C. P. Grey, Capturing metastable structures during high-rate cycling of $LiFePO_4$ nanoparticle electrodes, *Science*, **344**(6191), 1252817 (2014).
13. Y. Li, F. El Gabaly, T. R. Ferguson, R. B. Smith, N. C. Bartelt, J. D. Sugar, K. R. Fenton, D. A. Cogswell, A. L. D. Kilcoyne, T. Tyliszczak, M. Z. Bazant, and W. C. Chueh, Current-induced transition from particle-by-particle to concurrent intercalation in phase-separating battery electrodes, *Nat. Mater.*, **13**(12), 1149 (2014).
14. B. Orvananos, T. Ferguson, H.-C. Yu, M. Z. Bazant, and K. Thornton, Particle-Level Modeling of the Charge-Discharge Behavior of Nanoparticulate Phase-Separating Li-Ion Battery Electrodes, *J. Electrochem. Soc.*, **161**(4), A535 (2014).
15. B. Orvananos, R. Malik, H.-C. Yu, A. Abdellahi, C. P. Grey, G. Ceder, and K. Thornton, Architecture Dependence on the Dynamics of Nano-$LiFePO_4$ Electrodes, *Electrochim. Acta*, **137**, 245 (2014).
16. B. Orvananos, H.-C. Yu, A. Abdellahi, R. Malik, C. P. Grey, G. Ceder, and K. Thornton, Kinetics of nanoparticle interactions in battery electrodes, *J. Electrochem. Soc.*, **162**(6), A965 (2015).
17. T. Sasaki, Y. Ukyo, and P. Novák, Memory effect in a lithium-ion battery, *Nat. Mater.*, **12**, 569 (2013).
18. A. Van der Ven and M. Wagemaker, Effect of surface energies and nano-particle size distribution on open circuit voltage of Li-electrodes, *Electrochem. Commun.*, **11**(4), 881 (2009).
19. N. Meethong, H.-Y. Huang, W. C. Carter, and Y.-M. Chiang, Size-Dependent Lithium Miscibility Gap in Nanoscale $Li_{1-x}FePO_4$, *Electrochem. Solid-State Lett.*, **10**(5), A134 (2007).
20. D. A. Porter and K. E. Easterling, *Phase Transformations in Metals and Alloys, (Revised Reprint)*, CRC press (1992).
21. K. T. Lee, W. H. Kan, and L. F. Nazar, Proof of Intercrystallite Ionic Transport in $LiMPO_4$ Electrodes (M = Fe, Mn), *J. Am. Chem. Soc.*, **131**(17), 6044 (2009).
22. H.-C. Yu, B. Orvananos, S. Cronin, M. Z. Bazant, S. Barnett, and K. Thornton, Smoothed boundary simulation of electrochemical kinetics in $LiCoO_2$ cathode with a complex microstructure. In preparation.
23. H.-C. Yu, H.-Y. Chen, and K. Thornton, Extended smoothed boundary method for solving partial differential equations with general boundary conditions on complex boundaries, *Modell. Simul. Mater. Sci. Eng.*, **20**(7), 075008 (2012).
24. B. Orvananos Murguia, *Modeling and Simulation of Nanoparticulate Lithium Iron Phosphate Battery Electrodes*. PhD thesis, The University of Michigan (2014).
25. X. Zhang, M. van Hulzen, D. P. Singh, A. Brownrigg, J. P. Wright, N. H. van Dijk, and M. Wagemaker, Rate-Induced Solubility and Suppression of the First-Order Phase Transition in Olivine LiFePO 4, *Nano Lett.*, **14**(5), 2279 (2014).
26. J. S. Newman and C. W. Tobias, Theoretical analysis of current distribuion in poruous electrodes, *J. Electrochem. Soc.*, **109**(12), 1183 (1962).
27. L. Wang, F. Zhou, Y. Meng, and G. Ceder, First-principles study of surface properties of $LiFePO_4$: Surface energy, structure, Wulff shape, and surface redox potential, *Physical Review B*, **76**(16), 165435 (2007).
28. J. Xie, N. Imanishi, T. Zhang, A. Hirano, Y. Takeda, and O. Yamamoto, Li-ion diffusion kinetics in $LiFePO_4$ thin film prepared by radio frequency magnetron sputtering, *Electrochim. Acta*, **54**(20), 4631 (2009).
29. Y. Zhu and C. Wang, Galvanostatic Intermittent Titration Technique for Phase-Transformation Electrodes, *J. Phys. Chem. C*, **114**(6), 2830 (2010).
30. M. Takeuchi, Y. Kameda, Y. Umebayashi, S. Ogawa, T. Sonoda, S.-I. Ishiguro, M. Fujita, and M. Sano, Ion-ion interactions of $LiPF_6$ and $LiBF_4$ in propylene carbonate solutions, *J. Mol. Liq.*, **148**(2-3), 99 (2009).
31. J. Hofhaus and E. F. Van de Velde, Alternating-direction line-relaxation methods on multicomputers, *SIAM J. Sci. Comput.*, **17**(2), 454 (1996).
32. E. F. Van de Velde, *Concurrent Scientific Computing*, chapter 8, page 202. Springer-Verlag, New York, 1st edition (1994).
33. J. Cabana, J. Shirakawa, G. Chen, T. J. Richardson, and C. P. Grey, MAS NMR study of the metastable solid solutions found in the $LiFePO_4/FePO_4$ system, *Chem. Mater.*, **22**(3), 1249 (2010).
34. F. C. Strobridge, B. Orvananos, M. Croft, H.-C. Yu, R. Robert, H. Liu, Z. Zhong, T. Connolley, M. Drakopoulos, K. Thornton, and C. P. Grey, Mapping the inhomogeneous electrochemical reaction through porous $LiFePO_4$-electrodes in a standard coin cell battery, *Chem. Mater.*, **27**(7), 2374 (2015).
35. W. A. Paxton, Z. Zhong, and T. Tsakalakos, Tracking inhomogeneity in high-capacity lithium iron phosphate batteries, *J. Power Sources*, **275**, 429 (2015).